PON Monitoring Scheme Based on TGD-OFDR with High Spatial Resolution and Dynamic Range

ZHU Yidai[1], FAN Xinyu[2], ZHU Songlin[1], DONG Jiaxing[2], LI Guoqiang[1], HE Zuyuan[2]

(1. Wireline Product Planning Department, ZTE Corporation, Shanghai 201203, China;
2. School of Electronic Information and Electrical Engineering, Shanghai Jiao Tong University, Shanghai 200240, China)

DOI: 10.12142/ZTECOM.202504002

https://kns.cnki.net/kcms/detail/34.1294.TN.20251127.1332.002.html, published online November 27, 2025

Manuscript received: 2025-08-15

Abstract: Conventional optical time-domain reflectometry (OTDR) schemes for passive optical network (PON) link monitoring are limited by insufficient dynamic range and spatial resolution. The expansion of PONs, with increasing optical network units (ONUs) and cascaded splitters, imposes even more stringent demands on the dynamic range of monitoring systems. To address these challenges, we propose a time-gated digital optical frequency-domain reflectometry (TGD-OFDR) system for PON monitoring that effectively decouples the inherent coupling between spatial resolution and pulse width. The proposed system achieves both high spatial resolution (~0.3 m) and high dynamic range (~30 dB) simultaneously, marking a significant advancement in optical link monitoring.

Keywords: passive optical network (PON); time-gated digital optical frequency-domain reflectometry (TGD-OFDR); dynamic range; spatial resolution

Citation (Format 1): ZHU Y D, FAN X Y, ZHU S L, et al. PON monitoring scheme based on TGD-OFDR with high spatial resolution and dynamic range [J]. ZTE Communications, 2025, 23(4): 3 - 9. DOI: 10.12142/ZTECOM.202504002

Citation (Format 2): Y. D. Zhu, X. Y. Fan, S. L. Zhu, et al., "PON monitoring scheme based on TGD-OFDR with high spatial resolution and dynamic range," *ZTE Communications*, vol. 23, no. 4, pp. 3 - 9, Dec. 2025. doi: 10.12142/ZTECOM.202504002.

1 Introduction

Optical fiber, serving as a key transmission medium in communication links, is widely deployed in data communication networks owing to its advantages, including large bandwidth, low loss, strong anti-interference capability, low cost, material abundance, and longevity. Its deployment in backbone and metropolitan area networks has significantly increased data bandwidth while reducing operational costs.

Leveraging the abundant broadband resources of optical fiber, passive optical network (PON) technology has gained prominence since its inception. As a point-to-multipoint (P2MP) optical access technology, PON comprises an optical line terminal (OLT) at the central office, optical network units (ONUs) at user premises, and an optical distribution network (ODN). To ensure reliable operation of diverse PON services and enhance network stability, online monitoring of each PON link status is essential. This enables the prediction of potential optical link issues and facilitates timely corrective actions to guarantee service quality.

Traditional link monitoring primarily relies on optical time-domain reflectometry (OTDR)[1]. By launching optical pulses and analyzing the time-domain Rayleigh backscattered signal intensity, OTDR assesses link conditions, including attenuation, loss, and breaks. While achieving detection ranges of tens of kilometers, OTDR typically provides meter-scale spatial resolution.

However, a fundamental trade-off exists in OTDR between dynamic range and spatial resolution, constrained by the optical pulse width. The optical splitters inherent in PON architecture introduce additional losses, demanding a higher system dynamic range. Furthermore, the meter-scale spatial resolution of OTDR poses significant limitations in PONs with numerous terminals. These limitations impede the development of advanced PON monitoring solutions.

Several approaches have been proposed to address these challenges. For instance, tunable-wavelength OTDR[2] assigns distinct detection wavelengths to different ONUs. Alternatively, pulse coding techniques[3] assign unique codes to branch links and increase the effective probe power, thereby boosting the system dynamic range. Continuous-wave optical frequency-

This work was supported by ZTE and Shanghai Jiao Tong University Collaborative Laboratory under Grant No. IA20241205014.

domain reflectometry (OFDR) enables high-spatial-resolution PON monitoring by utilizing the unique Rayleigh backscatter spectral "fingerprint" of individual fibers beyond the splitter[4]. This approach offers high precision and can discern unique Rayleigh characteristics amidst overlapping signals from multiple fibers, serving as a powerful tool for real-time monitoring and individual event detection in PON. However, these studies[2-4] still fail to achieve simultaneous long-distance reach, high dynamic range, and high spatial resolution[5]. Furthermore, the number of ONUs that can be effectively monitored by these methods is limited. As the splitting ratio and number of cascaded splitters increase, the resulting higher insertion loss imposes stricter demands on the system dynamic range.

In a typical PON, the optical link needs to span up to 30 km. As the network gradually expands and the number of users increases, the use of two-stage 1:8 optical splitters to connect 64 ONUs has become a standard configuration. Considering such a PON structure featuring an optical fiber link exceeding 30 km and incorporating two stages of 1:8 optical splitters, as depicted in Fig. 1, a dynamic range of at least 26 dB is essential. This budget comprises 20 dB for the two-stage splitters and 6 dB for fiber transmission loss (0.2 dB/km @1 550 nm). Additionally, a spatial resolution finer than 0.3 m is required for detailed event monitoring. The high-spatial-resolution requirement renders OTDR inadequate. Conversely, long-distance OFDR detection is plagued by phase noise, limiting its achievable dynamic range. To meet these demanding requirements, we introduce a time-gated digital optical frequency-domain reflectometry (TGD-OFDR) system into PON. TGD-OFDR enables a long-distance link monitoring scheme achieving simultaneous high dynamic range and high spatial resolution. Since TGD-OFDR was first proposed by LIU et al. in 2015[6], many studies have been undertaken with the aim of improving the performance of the system. XIAO et al. employed a commercial integrated tunable laser assembly (ITLA) with a 100 kHz linewidth and introduced a frequency-domain reciprocal distortion phase noise compensation (FDRD-PNC) algorithm to improve the signal-to-noise ratio[7]. Consequently, a dynamic range of 21.8 dB and a spatial resolution of 3.48 m were achieved over a 50 km measurement fiber. Moreover, LUO et al. proposed a novel frequency-sweeping method by incorporating a frequency-shifting loop into the system to mitigate fading noise[8]. This scheme effectively suppressed fading noise without compromising spatial resolution, thereby enabling high-performance acoustic wave detection with high-frequency response. A spatial resolution of 1.43 m was achieved. For the inspection of PON structures, FONTAINE et al. employed a polarization-diversity coherent OFDR system to identify fibers and detect events in a 1:32 split PON[9]. They characterized an ODN spanning 21 km with a 1:32 split ratio, achieving a spatial resolution of less than 0.5 m and a dynamic range exceeding 35 dB.

In this study, we first provide a brief introduction to the principles of the TGD-OFDR system and the methodology for constructing a noise-incorporated simulation model. Subsequently, we establish the simulation model and analyze the impact of key parameters, including laser linewidth, pulse width, and splitting ratio, on the system's dynamic range.

Through simulations conducted under a 100 kHz laser linewidth condition, we demonstrate that the TGD-OFDR system meets the target specifications of 30 dB dynamic range and 0.3 m spatial resolution, validating its feasibility for high-precision distributed sensing applications.

2 Theory

TGD-OFDR launches a long-pulse frequency-swept probe into the fiber. By demodulating the returned Rayleigh backscatter signal via digital-domain heterodyne detection, it decouples spatial resolution from pulse width and mitigates the limiting impact of phase noise on the dynamic range. This section briefly introduces the basic principle of TGD-OFDR and establishes a preliminary simulation model incorporating phase noise.

Fig. 2 illustrates the basic structure of a TGD-OFDR system. An arbitrary waveform generator (AWG) generates a linear frequency-swept radio frequency (RF) pulse to drive an optical

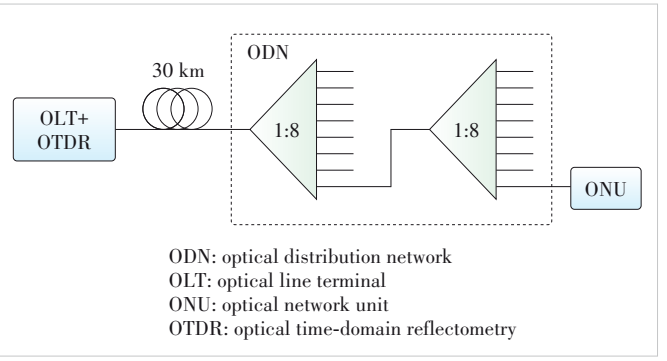

Figure 1. Structure of a typical passive optical network (PON)

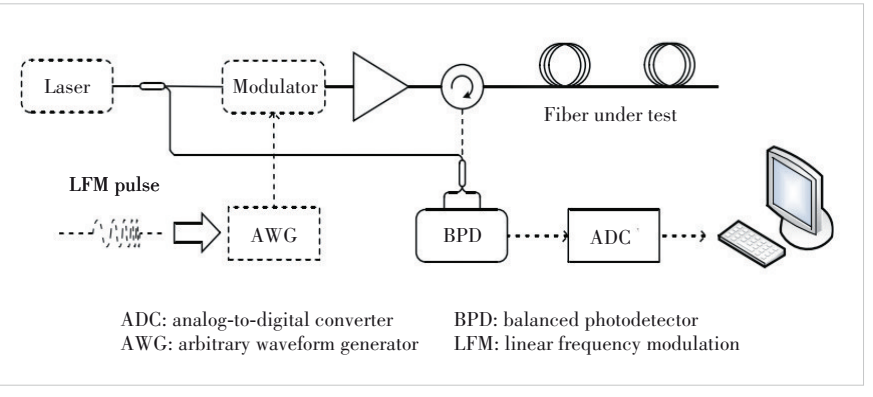

Figure 2. Basic structure of a time-gated digital optical frequency-domain reflectometry (TGD-OFDR) system

modulator, producing a linear frequency-swept optical pulse. The AWG-generated electrical signal is:

$$s(t) = W\left(\frac{t}{T_p}\right)e^{j\left[2\pi f_0 t + \pi\kappa t^2\right]} \quad (1),$$

where $W(\cdot)$ is the window function controlling the pulse shape over the pulse duration $[0, T_p]$, f_0 is the RF starting frequency, and κ is the frequency sweep rate. The resulting modulated optical field is:

$$E_P(t) = \sqrt{P_P}\,W\left(\frac{t}{T_p}\right)e^{j\left[\omega_c t + 2\pi f_0 t + \pi\kappa t^2\right]} \quad (2),$$

where P_P and ω_c are the power and frequency of the probe light (continuous-wave carrier), respectively. After Rayleigh backscattering occurs along the fiber, the total backscattered optical field returning to the receiver is:

$$E_R(t) = \sum_{i=1}^{N} E_i W\left(\frac{t-\tau_i}{T_p}\right)e^{j\left[\omega_c(t-\tau_i) + 2\pi f_0(t-\tau_i) + \pi\kappa(t-\tau_i)^2\right]} \quad (3),$$

where N is the total number of scattering points, E_i is the amplitude of the field from the i-th point (determined by the local Rayleigh scattering coefficient and accumulated fiber transmission loss up to that point), and τ_i is the round-trip time delay to the i-th scattering point. The returned backscattered light is combined with a portion of the original probe light (local oscillator, LO) and detected by a balanced photodetector (BPD). The BPD converts the optical interference into an electrical signal:

$$i(t) = \sum_{i=1}^{N} A_i W\left(\frac{t-\tau_i}{T_p}\right)\sin\left[2\pi f_0(t-\tau_i) + \pi\kappa(t-\tau_i)^2 - \omega_c\tau_i\right] \quad (4),$$

where A_i is the amplitude converted by the BPD.

A continuous digital replica of the frequency-swept signal is generated. This digital signal is mixed (multiplied) with the acquired electrical signal as shown in Eq. (4). This mixing process effectively down-converts the linear frequency-swept components into distance-dependent single-frequency signals. The sweep rate of this digital replica matches that of the optical probe signal, as illustrated in Fig. 3. The resulting beat frequency for each scattering point is directly proportional to its distance along the fiber. The amplitude of the signal component at frequency f_i reflects the local Rayleigh scattering coefficient at point i and the accumulated transmission loss from the beginning of the fiber to that point. Finally, applying a Fourier transform to the down-converted digital signal yields a frequency spectrum. The amplitude and frequency of each peak in this spectrum correspond to the scattering strength and location, respectively, of each point along the optical fiber, thus providing the distributed Rayleigh backscatter profile.

The preceding derivation neglects phase noise. However, for practical simulation, time discretization is required. Consequently, we establish the simulation model as follows. The sensing fiber is divided into N discrete scattering units, each of length L_w. Computational constraints prevent setting L_w to be extremely small (i.e., much smaller than the incident optical wavelength λ). However, provided L_w is much smaller than the spatial extent (coverage length) of the detection pulse, the statistical properties of the Rayleigh backscatter remain valid. Owing to inherent non-uniformities in the fiber drawing process and potential variations in temperature and strain along the fiber, the refractive index n_i within each scattering unit i is not constant. The average core refractive index is typically 1.45. Each scattering unit is represented by a single effective scattering point, from which all scattered light originating within that unit is assumed to emanate. The position of the scattering point within its unit is defined by an offset δL_{wi}, measured from the unit's input end. These offsets are independent and identically distributed (i.i.d.) random variables, each uniformly distributed over $[0, L_w)$. The Rayleigh scattering coefficient for each scattering point is also modeled as an i.i.d. random variable with a uniform distribution. The round-trip time delay τ_i for light propagating from the fiber input end to the i-th scattering point and back is given by:

$$\tau_i = \frac{L_w\sum_{x=1}^{i-1} n_{1x} + \delta L_{wi} n_{1i}}{c} \quad (5).$$

Therefore, the backscattered field in Eq. (3) can be expressed as:

$$E_R(t) = \sum_{i=0}^{N-1}\sqrt{\gamma_i}\sqrt{\alpha_i}\,E_P(t-\tau_i) \quad (6),$$

where α_i is the loss coefficient of the scattered light from the

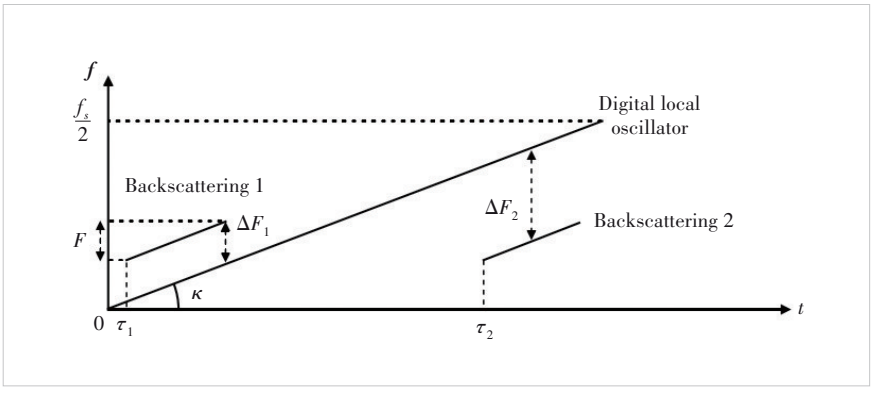

Figure 3. Schematic diagram of digital domain frequency-swept signal

i-th point along the entire optical path:

$$\alpha_i = \left(10^{\frac{L_w \alpha}{10}}\right)^{2i} \tag{7},$$

where α is the unit loss of optical fiber, normally taken as 0.2 dB/km@1 550 nm.

The phase noise $\phi(k)$, arising from the laser's finite linewidth, is modeled as a Wiener process affecting the instantaneous electric field of the probe light. Its increment $\phi(k-k_2)-\phi(k-k_1)$ follows a normal distribution with a mean value of 0 and a variance of $2\pi\Delta\nu(k_2-k_1)T_s$, where $\Delta\nu$ is the linewidth. By generating k independent and identically distributed random variables Φ_n following $N(0, 2\pi\Delta\nu T_s)$ and accumulating them, the phase noise can be obtained:

$$\phi(k) = \sum_{n=1}^{k} \Phi_n \tag{8}.$$

By substituting the phase noise into Eqs. (2) and (3), and revising Eq. (4) according to the distances of scattering points in the discrete case, we obtain:

$$i(k) = \eta(k) + R \cdot \sum_{i=0}^{N-1} \sqrt{\gamma_i}\sqrt{\alpha_i} \cdot s(k-\tau_i)\, e^{j[-\omega_c \tau_i + \phi(k-\tau_i) - \phi(k)]} \tag{9},$$

where $R = 2G \cdot R \cdot \sqrt{P_L}\sqrt{P_P}$, in which G is the gain of the BPD. Since the BPD gain amplifies both the signal and noise equally, it does not affect the signal-to-noise ratio (SNR). Therefore, in the simulation, we set the BPD gain to unity (i.e., 1) for simplified analysis without loss of generality. R is the responsivity of the BPD, which is set to 0.9 A/W in the simulation. The system noise, denoted by η, incorporates the effects of thermal noise, shot noise and amplified spontaneous emission (ASE) noise. Eq. (9) can be rewritten in the form of convolution[10]:

$$i(k) = \eta(k) + R \cdot [s'(k) \otimes h(k)] \cdot e^{-j\phi(k)} \tag{10},$$

where $s'(k) = s(k) \cdot e^{j\phi(k)}$, which implies that the phase noise of the laser is imposed on the phase of the electrical signal; $h(k)$ represents the impulse response of the optical fiber:

$$h(k) = \sqrt{\gamma_k}\sqrt{\alpha_k}\, e^{j[-\omega_c \cdot \frac{L_w \sum_{i=1}^{k-1} n_{1i} + \delta L_{wk} n_{1k}}{c}]} \tag{11}.$$

First, the system bandwidth B is set according to the total sampling rate of the simulation model and its corresponding sampling time interval T_s. The length of the optical fiber scattering unit L_w is defined as $cT_s/2n$. The total fiber length is set, and the total number of scattering points N is calculated. Finally, the position distribution, scattering rate distribution and attenuation distribution of the scattering points are defined according to Eqs. (5) and (7). These distributions are substituted into Eq. (11) to obtain the optical fiber impulse response $h(k)$.

Subsequently, we generate the frequency-swept pulsed light. First, a single-frequency continuous light is generated according to the incident light wavelength and the speed of light. According to Eq. (8), the phase noise corresponding to the total duration of the optical signal is generated and imposed on the phase of the optical signal. Then we generate the corresponding window signal mask $W(\cdot)$ based on the rise time, fall time, and acousto-optic modulator (AOM) extinction ratio. The above information is substituted into Eq. (1) to generate the frequency-swept electrical signal $s(k)$.

Finally, we convolve the frequency-swept electrical signal $s(k)$ with the optical fiber impulse response $h(k)$, and calculate the amplitude coefficient R resulting from the optical power, PD gain, and responsivity. Then, according to Eq. (10), we superimpose the phase noise term and other noise terms $\eta(k)$, and finally obtain the photocurrent from coherent reception.

3 Simulation

In conventional TGD-OFDR systems, the frequency-swept pulse is directly applied to the AOM. However, due to the limitations in the operating frequency and bandwidth of the AOM, the frequency sweep range of the system cannot exceed hundreds of MHz. To achieve a wide-range frequency sweep, we have modified the system architecture as illustrated in Fig. 4. A continuous frequency-swept optical signal is modulated via an in-phase/quadrature (IQ) modulator, followed by an injection-locked scheme for amplification and filtering. Subsequently, the AOM is utilized to extract the pulsed signal. After being amplified by the Erbium-doped fiber amplifier (EDFA), the probe signal is injected into the fiber under test for sensing, and is received with the local signal through a polarization diversity receiver (PDR). In this scheme, the AOM functions solely as a high-speed optical switch. The overall frequency sweep range of the system is determined by the bandwidth of the modulator and the performance of the AWG, thereby substantially elevating the upper limit of the sweep range.

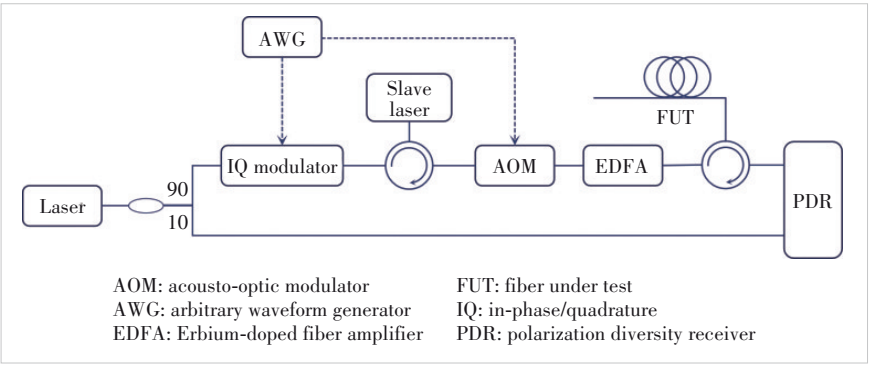

Figure 4. Structure of a simulated time-gated digital optical frequency-domain reflectometry (TGD-OFDR) system

The simulation platform was developed within the MATLAB environment. The key simulation parameters are shown in Table 1.

For computational efficiency in the simulation, the fiber link was first modeled as three concatenated 1 km fiber segments with 10 dB insertion loss at each splicing point to emulate the power attenuation caused by optical splitters in practical deployments; 100 independent measurements were averaged to enhance system performance. Using these parameters, the dynamic range performance was simulated for different laser linewidths (100 Hz to 1 MHz), pulse widths (10 μs to 100 μs), and splitting ratios (1:99, 10:90, and 50:50), respectively.

1) Linewidth

The incident optical power was fixed at 0 dBm and the pulse width at 100 μs. The laser linewidth was varied sequentially from 100 Hz to 1 MHz, increasing by a factor of ten at each step. Representative Rayleigh spectra are shown in Fig. 5. The corresponding dynamic ranges are compiled in Table 2. It is evident that a tenfold increase in laser linewidth results in an approximate 5 dB decrease in the dynamic range.

2) Pulse width

The laser linewidth was fixed at 1 kHz, the source optical power at 0 dBm, and the splitting ratio between the LO path and the sensing path at 10:90. The pulse width was varied from 10 μs to 100 μs. Rayleigh spectra obtained for different pulse widths are shown in Fig. 6. The resulting dy-

Table 1. Key parameters for the proposed TGD-OFDR simulation model

Parameter	Value
Sampling rate	8 GS/s
Wavelength	1 550 nm
Speed of light	299 792 458 m/s
Extinction ratio (AOM)	40 dB
Operating frequency (AOM)	80 MHz
Gain (EDFA)	30 dB
Detection optical power	0 dBm
Fiber attenuation	0.2 dB/km

AOM: acousto-optic modulator
EDFA: Erbium-doped fiber amplifier
TGD-OFDR: time-gated digital optical frequency-domain reflectometry

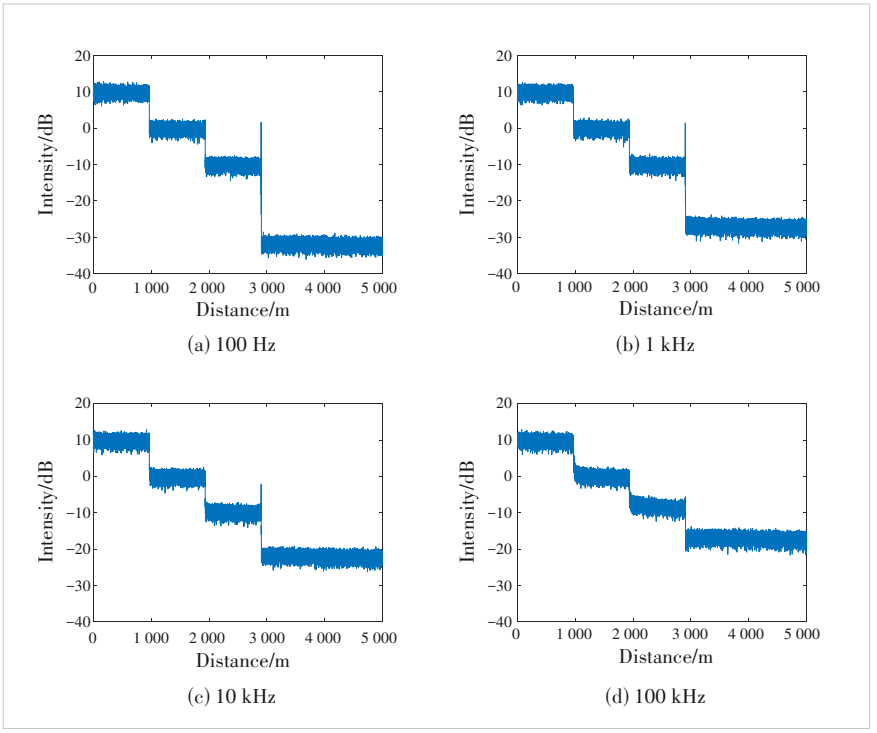

Figure 5. Simulated Rayleigh spectra with different laser linewidths

Table 2. Statistics of dynamic ranges with different linewidths

Linewidth	100 Hz	1 kHz	10 kHz	100 kHz	1 MHz
Dynamic range/dB	44.527 2	39.921 2	34.619 2	29.396 1	23.841 6

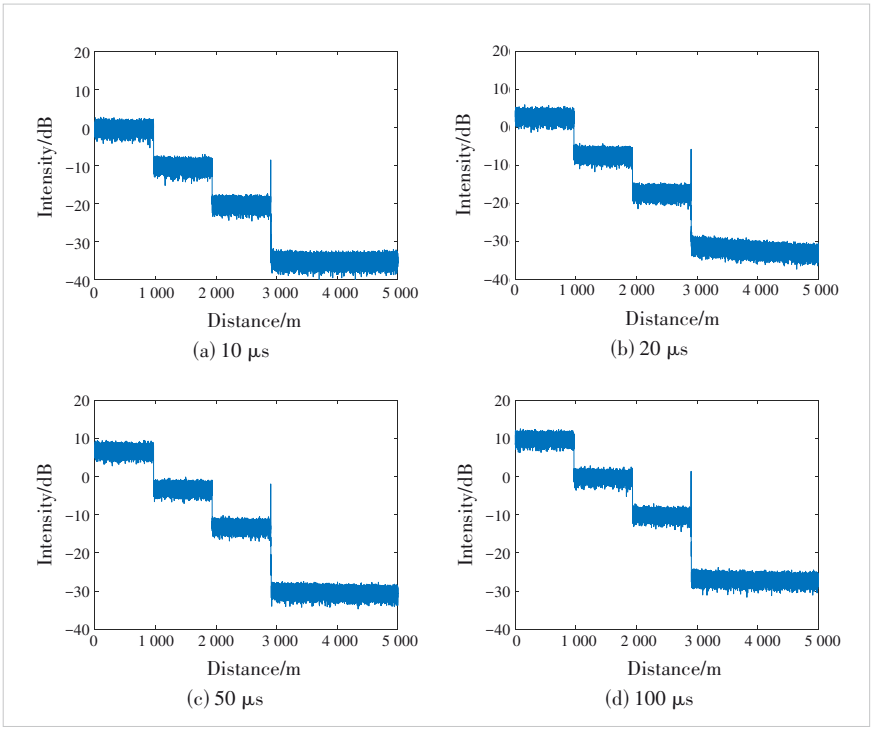

Figure 6. Simulated Rayleigh spectra with different pulse widths

Table 3. Statistics of dynamic ranges with different pulse widths

Pulse width/μs	10	20	50	100
Dynamic range/dB	33.014 6	35.234 8	37.152 3	39.921 2

namic ranges are compiled in Table 3. As the pulse width increases, the system's dynamic range improves. This is because TGD-OFDR shares similarities with OTDR, which utilizes pulsed light for detection; thus, increasing the pulse power enhances the dynamic range.

3) Splitting ratio

Adjusting the splitting ratio can effectively increase the LO power, thereby improving the system SNR. With the incident optical power fixed at 0 dBm, the dynamic range was simulated for different splitting ratios. The results are shown in Fig. 7. Increasing the splitting ratio (directing more power to the LO) significantly enhances the dynamic range by increasing the LO power. Common splitting ratios achievable with standard couplers are listed in Table 4. However, the improvement in this dynamic range is limited. When the LO power becomes excessive, the shot noise it generates begins to dominate over the thermal noise, and the system SNR becomes limited solely by the sensing path power. Conversely, increasing the splitting ratio reduces the sensing path power, establishing a trade-off between the LO power and sensing path power. Therefore, the simulations indicate that a splitting ratio of 10:90 yields the optimal dynamic range.

Finally, simulations were conducted with the following optimized parameters: an incident optical power of 10 dBm, a splitting ratio of 1∶9, a pulse width of 100 μs, and 100 averages. We extended the fiber under test to three concatenated 10 km fiber segments with parameters closer to those of a real-world PON, while maintaining the two-stage splitter configuration. The simulation results are shown in Fig. 8. The total fiber length of 30 km corresponds to an attenuation loss of 6 dB. Combined with the 20 dB transmission loss of the two-stage splitters, the overall link loss reaches 26 dB. The pulse width is set to 100 μs, and the sweep range is set from 100 MHz to 1 100 MHz. Under the condition of linewidths of 1 kHz and 100 kHz, the total dynamic

Table 4. Statistics of dynamic ranges with different splitting ratios

Splitting ratio	1:99	10:90	50:50
Dynamic range/dB	26.004 2	30.182 8	31.477 6

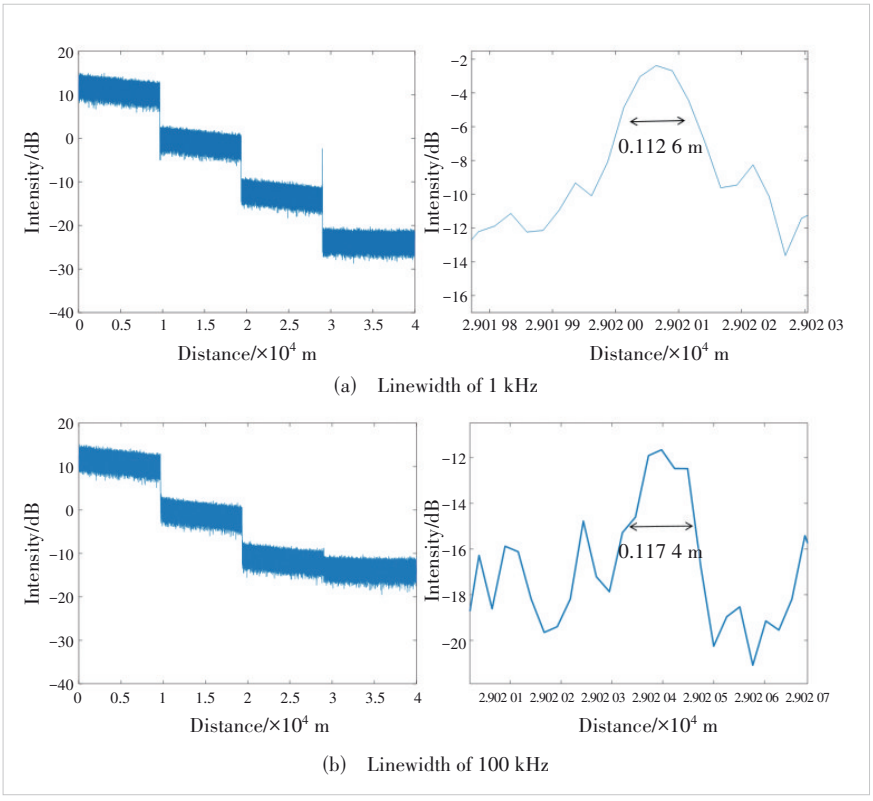

Figure 8. Simulated Rayleigh spectra of a 30 km fiber under test with different laser linewidths and calculated spatial resolution

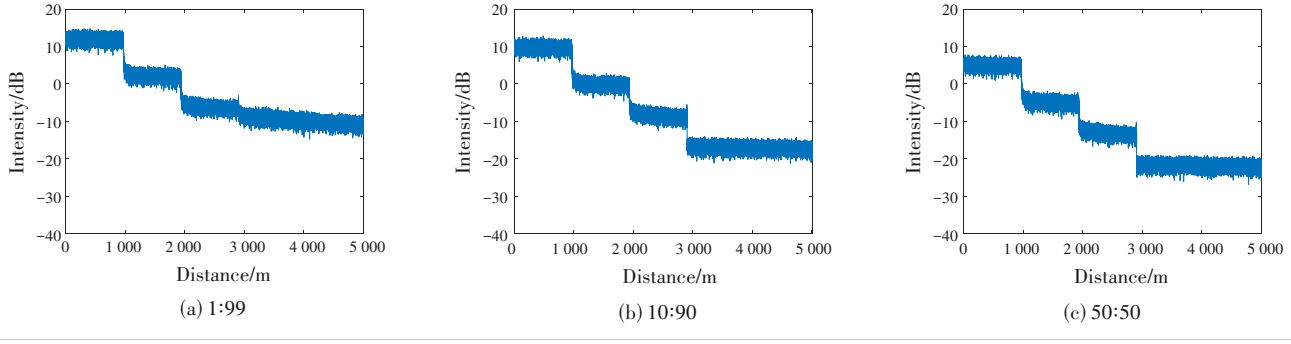

Figure 7. Simulated Rayleigh spectra with different splitting ratios

range reaches 34.013 5 dB and 28.157 0 dB, and the spatial resolution (using the 3 dB width of the end reflection peak as the benchmark) is 0.112 6 m and 0.117 4 m. These simulations demonstrate that the system achieves a sensing distance of 30 km and a spatial resolution of less than 0.3 m, thereby meeting the requirements for high-spatial-resolution and high-dynamic-range PON monitoring.

4 Conclusions

Simulation results demonstrate that the TGD-OFDR system overcomes key limitations of conventional OTDR, specifically insufficient incident optical pulse power and the inherent constraint linking spatial resolution to pulse width. While maintaining high spatial resolution, the system achieves a significantly enhanced dynamic range. Compared to conventional OTDR systems, which require hundreds of thousands of averages to achieve a dynamic range of 15 dB with a spatial resolution on the order of meters, the TGD-OFDR technique achieves superior spatial resolution (<0.3 m) and dynamic range (>25 dB) with significantly fewer averages (<500 times) and a much faster measurement rate. When applied to PONs, the system enables the monitoring of multi-stage optical splitters, supporting a larger number of ONUs over an extended reach while delivering a superior SNR. For a representative scenario involving two cascaded 1:8 splitters (imposing a minimum attenuation of ~20 dB), the TGD-OFDR-based PON monitoring system achieves a sensing distance of 30 km, a spatial resolution below 0.3 meters, and a dynamic range approaching 30 dB. This advancement holds significant potential for both fundamental research and the practical realization of intelligent digital PONs.

References

[1] CHAMPAVÈRE A. New OTDR measurement and monitoring techniques [C]//Proc. Optical Fiber Communication Conference. OSA, 2014. DOI: 10.1364/ofc.2014.w3d.1
[2] OZAWA K. Field trial of in-service individual line monitoring of PONs using a tunable OTDR [C]//Proc. Fourteenth International Conference on Optical Fiber Sensors. SPIE, 2000: 101 – 104. DOI: 10.1117/12.2302161
[3] FATHALLAH H, RAD M M, RUSCH L A. PON monitoring: periodic encoders with low capital and operational cost [J]. IEEE photonics technology letters, 2008, 20(24): 2039 – 2041. DOI: 10.1109/LPT.2008.2006060
[4] FONTAINE N K, MAZUR M, PUTTNAM B J, et al. Ultra-high resolution and long-range OFDRs for characterizing and monitoring Hollow-core DNANFs [C]//Proc. Optical Fiber Communication Conference (OFC). Optica Publishing Group, 2025: 101 – 104. DOI: 10.1364/ofc.2025.th4d.6
[5] ZHOU X, ZHANG F D, SUN M M, et al. A modified optical coding monitoring scheme in PON with electronic decoding processing [J]. IEEE communications letters, 2013, 17(9): 1849 – 1851. DOI: 10.1109/LCOMM.2013.090213.131501
[6] LIU Q W, FAN X Y, HE Z Y. Time-gated digital optical frequency domain reflectometry with 16-m spatial resolution over entire 110-km range [J]. Optics express, 2015, 23(20): 25988. DOI: 10.1364/oe.23.025988
[7] XIAO Z Y, PAN Y C, CHEN J G, et al. High-performance and low-cost distributed acoustic sensor with phase noise compensation [C]//Proc. Asia Communications and Photonics Conference (ACP) and International Conference on Information Photonics and Optical Communications (IPOC). IEEE, 2024. DOI: 10.1109/ACP/IPOC63121.2024.10810028
[8] LUO Y M, LIU Q W, LIU C Z, et al. A fading noise suppression method based on frequency-shift loop in TGD-OFDR system [C]//Proc. Asia Communications and Photonics Conference (ACP) and International Conference on Information Photonics and Optical Communications (IPOC). IEEE, 2024. DOI: 10.1109/ACP/IPOC63121.2024.10810004
[9] DALLACHIESA L, MAZUR M, IANNONE P, et al. Coherent OFDR-based individual fiber identification and event detection over a 21-km passive optical distribution network with a 1:32 split [C]//2025 Optical Fiber Communications Conference and Exhibition (OFC). OPTICA, 2025: 1 – 3
[10] CHEN D, LIU Q W, HE Z Y. Phase-detection distributed fiber-optic vibration sensor without fading-noise based on time-gated digital OFDR [J]. Optics express, 2017, 25(7): 8315 – 8325

Biographies

ZHU Yidai received his BS degree in optoelectronic science and engineering from the University of Electronic Science and Technology of China in 2020, and PhD degree in information and communication engineering from Shanghai Jiao Tong University, China in 2025. He joined the Wireline Product Planning Department, ZTE Corporation in 2025. His research interests include optical communications and optical sensing applications.

FAN Xinyu (fan.xinyu@sjtu.edu.cn) received his BS and MS degrees in applied physics from Shanghai Jiao Tong University, China in 2000 and 2003, respectively, and PhD degree in electrical engineering from the University of Tokyo, Japan in 2006. In the same year, he joined the NTT Access Network Service Systems Laboratories, Japan, where his research interests included optical reflectometry and optical measurement. Since 2012, he has been with the Department of Electrical Engineering, Shanghai Jiao Tong University, where he is currently a Professor. His research interests include optical fiber sensing technology, optical fiber measurement, and fiber-related applications.

ZHU Songlin received his MS degree in theoretical physics from Hangzhou University, China in 1998 and PhD degree in electronic science and technology from Zhejiang University, China in 2001. He joined the Wireline Product Planning Department, ZTE Corporation in 2001. His research interests include FTTx technology for optical communications and OTDR technology for optical sensing applications.

DONG Jiaxing received his BS degree in electronic information and electrical engineering from Shanghai Jiao Tong University, China in 2024. He is currently working toward the master's degree at the School of Integrated Circuits, Shanghai Jiao Tong University. His research focuses on optical fiber sensors.

LI Guoqiang received his BS degree in electronic information engineering from Wuhan University, China in 2019 and PhD degree in electromagnetic field and microwave technology from Fudan University, China in 2024. He joined the Wireline Product Planning Department, ZTE Corporation in 2024. His research interests include digital signal processing for optical communications and OTDR technology for optical sensing applications.

HE Zuyuan received his BS and MS degrees in electronic engineering from Shanghai Jiao Tong University, China in 1984 and 1987, respectively, and PhD degree in photonics from the University of Tokyo, Japan in 1999. He joined CIENA Corporation, USA in 2001, as a Lead Engineer, where he headed the optical testing and optical process development group. He returned to the University of Tokyo as a Lecturer in 2003, and then became an Associate Professor in 2005 and a Full Professor in 2010. He is now a Chair Professor and Head of the Department of Electronic Engineering at Shanghai Jiao Tong University. His current research interests include optical fiber sensors, specialty optical fibers, and optical interconnects.